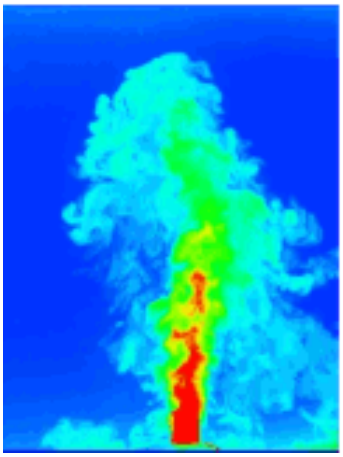

Journal of Turbulence
Publication details, including instructions for authors and subscription information:
http://www.informaworld.com/smpp/title~content=t713665472

Experimental study on a jet issuing from an elliptic nozzle with cylindrical tabs

S. B. Verma[a]; S. Sudhakar[a]; L. Venkatakrishnan[a]
[a] Experimental Aerodynamics Division, National Aerospace Laboratories, Council of Scientific and Industrial Research, Bangalore, India

First published on: 15 June 2010

To cite this Article Verma, S. B. , Sudhakar, S. and Venkatakrishnan, L.(2010) 'Experimental study on a jet issuing from an elliptic nozzle with cylindrical tabs', Journal of Turbulence, Volume 11, Art. No. N 20,, First published on: 15 June 2010 (iFirst)
To link to this Article: DOI: 10.1080/14685248.2010.490221
URL: http://dx.doi.org/10.1080/14685248.2010.490221

Journal of Turbulence
Vol. 11, No. 20, 2010, 1–24

Experimental study on a jet issuing from an elliptic nozzle with cylindrical tabs

S.B.Verma*, S. Sudhakar and L.Venkatakrishnan

Experimental Aerodynamics Division, National Aerospace Laboratories, Council of Scientific and Industrial Research, Bangalore 560 017, India

(*Received 21 December 2009; final version received 23 April 2010*)

An elliptic jet with mixing tabs was investigated using the digital particle-image-velocimetry and two-component hotwire anemometry. Two tabs of cylindrical configuration were placed on the minor-axis sides of a 2:1 elliptic nozzle. Because of their sideways pressure-relieving effect, a cylindrical tab relieves the constraint on the flow relative to a thin tab with flat surfaces which can have important implications on tab drag reduction but with similar mixing characteristics. Measurements were made for a jet exit velocity of 20 m s^{-1} and for Reynolds number based on the nozzle equivalent diameter (D_e) of 5.08×10^4. Furthermore, the effect of tab height ($h/d = 1.0$ and 1.67) is also investigated. The study shows the evolution of a mushroom structure behind each tab that distorts the jet flow into a two-finger structure. The tab wake mainly comprises of base vortices and tip vortices that are enveloped from the sides by spanwise vortical structures. While the strong upwash from the base vortices causes an inward penetration of the wake inhibiting the jet growth along the minor-axis plane, the net flow induced by the vortices shed from the tab free-end and the base region promotes jet growth along the major-axis plane, thereby preventing axis-switching. The combined effect of the above induces a rapid inward and lateral growth of spanwise generated vortices which begin to show at some downstream distance along the jet centreline that marks the end of the jet potential-core and the beginning location of jet-core bifurcation. An increase in the tab height shifts this location further upstream and promotes still higher jet growth along the major-axis plane. The intense initial mixing process initiated by the cylindrical tabs causes a rapid increase in the wake width and a subsequent increase in the overall turbulent intensity.

Keywords: cylindrical tabs; base vortex; spanwise vortex; axis-switching; jet-core bifurcation

Nomenclature

d	diameter of the cylindrical tab, mm
D_e	equivalent diameter of the elliptic nozzle, mm
h	height of the tab, mm
Re_{De}	Reynolds number based on equivalent diameter of the elliptic nozzle
Re_d	Reynolds number based on the diameter of the cylindrical tab
u'/U_e	non-dimensional streamwise velocity fluctuation
$u'v'/U_e^2$	Reynolds shear stress

*Corresponding author. Email: sbverma@ead.cmmacs.ernet.in

ISSN: 1468-5248 online only

DOI: 10.1080/14685248.2010.490221
http://www.informaworld.com

U_e	mean streamwise jet exit velocity, m s^{-1}
U	local mean streamwise jet velocity, m s^{-1}
V	local mean jet velocity along Y-direction, m s^{-1}
X	streamwise distance along the jet centerline, mm
Y	cross-stream distance along minor-axis plane, mm
Z	cross-stream distance along major-axis plane, mm
$Y_{0.5}$	jet half-width growth along minor-axis plane, mm
$Z_{0.5}$	jet half-width growth along major-axis plane, mm
w_y	cross-stream vorticity along minor-axis plane, s^{-1}
w_z	cross-stream vorticity along major-axis plane, s^{-1}
δ_{mi}	jet exit shear-layer thickness along minor-axis plane, mm
δ_{mj}	jet exit shear-layer thickness along major-axis plane, mm

1. Introduction

Mixing enhancement in jet flows is of paramount importance in many engineering applications and therefore has been the subject of continuing research. In recent years, increasing efforts have been devoted towards investigating various methods of attaining better mixing and to understand the fundamental fluid physics involved. Jet characteristics are known to be closely related to the dynamics of shear flow originating at the nozzle exit, and hence are strongly affected by the shape of the nozzle from which they issue [1]. As a result, frequently the jet geometry is dictated by the nature of application.

One of the most commonly used methods of shear flow control in jets is the use of nozzles with non-circular exit cross-sections, which significantly changes the jet flow development as compared with a jet issuing from a circular nozzle. Studies on jets issuing from non-circular nozzle geometries such as triangular [2], square [3], rectangular [4,5] and elliptic [6–9] have been reported in the past. The motivation behind each of these studies has been the enhanced entrainment and mixing characteristics. One of the earliest works reported on elliptic jets [10] studied the differing growth rates along the major- and minor-axis planes. Later studies on the entrainment characteristics of elliptic jets [6] found that the initial instability mode in these jets is strongly linked to the thinnest jet momentum thickness around the nozzle circumference. Further studies [7] on coherent structures of elliptic jets revealed that the jet undergoes a three-dimensional deformation process associated with the azimuthal distortion and bending of the elliptic vortex ring wherein ambient mass is brought in towards the jet-centreline along the major-axis side, and jet mass is thrown out along the minor-axis side. This non-uniform self-induction process results in enhanced mixing between the jet and the ambient irrotational mass [6–8]. As a result, the jet undergoes axis-switching, entrains more fluid and spreads faster in the minor-axis plane as was also observed for rectangular jets [4,5]. The behaviour of coherent structures was also found to be strongly affected by initial flow conditions such as the jet aspect ratio, initial momentum thickness, excited or unexcited, and therefore could be manipulated [7].

Other than the use of non-circular nozzle exit geometries, means were also explored to interfere with the shear-layer growth by the use of intrusive devices in the nozzle periphery. The streamwise vortices generated from such mixing devices provided the necessary secondary instabilities and were found to alter the flow-field development significantly. Gross distortions of the jet structure were observed using tabs, both in subsonic [11–15] and supersonic regimes [16–20]. The introduction of rectangular tabs in the nozzle periphery (blockage area of 1–2% per tab) was observed to introduce circumferential variations in

the jet flow development by splitting the jet into two high-velocity regions on either side of the diameter joining the two tabs [12]. These gross distortions resulted in increased jet entrainment. However, most of the earlier studies are based on tabs fabricated from flat plates and cut in the shape of rectangular or triangular configurations. Such variations in tab geometries [15] and their inclination [21] with respect to the jet axis have been found to strongly govern the initial vortex dynamics. Individual studies on the flow past a trapezoidal tab [22,23] and a finite-length cylinder [24–26] mounted on a flat plate have also been carried out. However, the flow development downstream of a finite-length cylinder mounted on a flat plate (no-slip condition) changes significantly when such a cylindrical configuration is placed in a jet flow (slip condition) at the nozzle exit. The focus of the present work was therefore to study the flow structure development behind a tab of cylindrical configuration in a jet flow and, thereafter, its effect on the overall jet flow development.

Most of the earlier studies report using thin tabs with flat front and back surfaces. Such a tab configuration presents a constraint to the oncoming flow, thereby causing significant changes in local velocity and pressure. On the other hand, owing to their sideways' 'pressure-relieving' effect, the flow past tabs with cylindrical configuration is more relaxed and somewhat 'relieved' in comparison to the flow past thin tabs with flat front and back surfaces. As a result, cylindrical tabs can have important implications on tab drag reduction (as compared to conventionally used tab designs) which may otherwise contribute approximately 1–1.5% towards overall thrust loss. The flow development from jets with tabs of cylindrical configuration has not been reported before and was the main objective of this study. Two such tabs are placed on the minor-axis sides (projecting normally into the flow at the nozzle exit) of a 2:1 elliptic nozzle. Furthermore, the effect of tab height is also investigated. A comparison is made with the jet issuing from a 2:1 elliptic nozzle without tabs, hereafter referred to as the 'plain jet'. A two-component digital particle image velocimetry (DPIV) is used to study the gross flow-field features (in the $X - Y$ and $X - Z$ planes) in view of its capability to acquire large ensembles of instantaneous data. The availability of simultaneous whole field velocity data allows the computation of correlations, thus enabling a better understanding of the flow structures. A two-component hotwire probe (X-wire) was also used for detailed grid measurements in the $Y - Z$ plane of the jet in (i) the tab wake region and (ii) the jet half-plane at various axial locations to study the flow structure development behind the tab and its effect on the overall jet flow development in the absence and presence of tabs, respectively.

2. Experimental set-up and procedure

2.1. *Set-up and test models*

Experiments were carried out to investigate the jet flow development from a 2:1 elliptic nozzle, with and without tabs, as shown in Figure 1. The nozzle has a circular section of 203 $\pm$ 0.1 mm diameter, smoothly contoured to an elliptic section ($2a = 54 \pm 0.1$ mm and $2b = 27 \pm 0.1$ mm) over a length of 300 ± 0.1 mm, where $2a$ and $2b$ are the major- and minor-axis diameters, respectively. The equivalent diameter (D_e) of the elliptic nozzle is 38 ± 0.2 mm. The measurements are carried out at a nominal jet exit velocity (U_e) of 20 ± 0.5 m s^{-1} and the Reynolds number based on the equivalent diameter of the jet (D_e) is $5.08 \pm 0.05 \times 10^4$. Two cylindrical tabs ($d = 3 \pm 0.1$ mm) are placed in the minor-axis plane of a 2:1 elliptic nozzle to modify the initial jet development in this plane. The main emphasis of the study was to look into the flow physics involved when (a) a tab of cylindrical configuration is used in a jet issuing from an elliptic nozzle and (b) tab height is varied ($h/d = 1.0$ and 1.67 with corresponding total percentage blockage of 1.6 and 2.6, respectively).

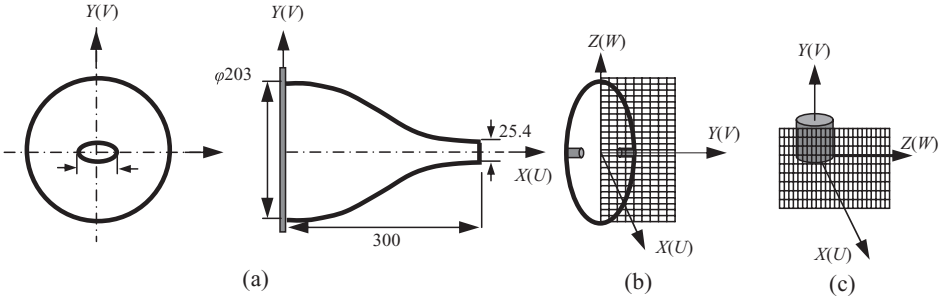

Figure 1. A schematic diagram of (a) the 2:1 elliptic nozzle, (b) tab placement ($\varphi = 90$ deg.) and grid measurement plane for overall jet development study, and (c) near-wake grid measurement plane (all dimensions are in mm).

2.2. *Instrumentation*

A 400 mJ, dual cavity Nd: YAG laser from *Spectra Physics*, capable of pulsing at 15 Hz was used as the light source for PIV measurements. A light sheet of over 200 ± 0.1 mm width, 1 mm thickness was generated using a set of spherical and cylindrical lenses, as shown in Figure 2(a). A Kodak ES 1.0 PIV camera of 1008(H) × 1018(V) pixels with a 50 mm Nikon lens was used for recording the particle images. The synchronization of the laser pulsing with camera and also the grabbing of the images were carried out using *IDT-1,000 controller* from *IDT* systems interfaced to a PC via a high-speed PCI link. Image acquisition and processing were carried out using *IDT proVISION*® software that operates in Windows 2000 platform on a dual Xeon processor workstation. A laser pulse interval of 25 μs results in a particle image displacement of about 2.5 pixels for the maximum velocity in the jet. The spatial resolution of PIV was about 5 × 5 mm when the images were processed using 24 pixels interrogation cells without overlap. However, this resolution being low, the results presented here are with 50% overlap. Additionally, in order to better emphasize the flow field, the data were then interpolated by a factor of two in order to produce smooth velocity fields. For the estimation of ensemble-averaged quantities, 1200 frames of data from each set were used. The PIV data were analysed on a grid of 125 × 125 points. The flow in the jet is seeded both internally and externally with fine droplets of fog fluid generated from a locally made nebulizer that produces seed particles of the order of 5 μm diameter. PIV recordings were carried out up to about 6 equivalent diameters spanning an area of 230 ± 0.1 mm^2.

The ability of the seeding particles to track the jet flow was checked by evaluating the Stokes number (*Stk*), which is defined as $Stk = \tau_{particle}/\tau_{flow}$, where $\tau_{particle}$ and τ_{flow} are the particle and jet flow timescales, respectively. The Stokes number, *St*, is a measure of particle inertia and represents the ratio of the particle response time to characteristic flow timescale [21]. As $St \to 0$, the particles and fluid trajectories are equivalent. For high fidelity of the fluid velocity measurement, it is desirable to have a very low Stokes number. The particle timescale was calculated using $\tau_{particle} = \rho D^2/18\mu$, where ρ and D are the density and diameter of the seed particle, respectively, while μ is the dynamic viscosity of air. The timescale of the jet flow was calculated using $\tau_{flow} = \delta/U_e$, where δ and U_e are the jet exit shear-layer thickness and the jet centreline exit velocity in the streamwise direction, respectively. On the basis of these experimental conditions, the Stokes number was found to be approximately $Stk = 0.9382$. Figure 2(b) shows a comparison of the centreline velocity decay for plain jet using hotwire data and that extracted from PIV measurements. It can be seen that although the Stokes number in the present measurements is relatively large [27], the

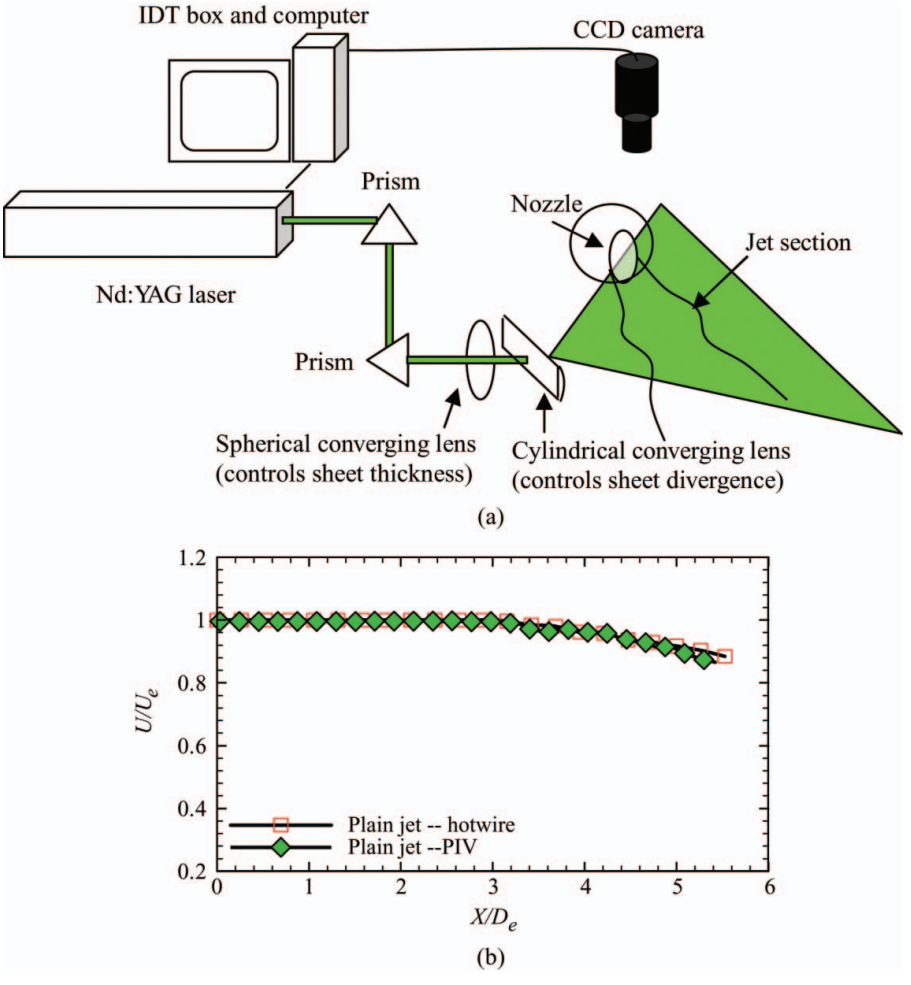

Figure 2. (a) A schematic diagram of the PIV optical set-up used for the present experiments and (b) comparison of centerline velocity (U/U_e) decay for the plain elliptic jet using hotwire and PIV measurements.

results show a good agreement between hotwire and PIV measurements. The uncertainty analysis in PIV measurements based on the method of Lourenco and Krothapalli [28] indicates that the errors of the determined velocity vectors are about $\pm 1.5\%$ of the actual velocity components.

Hotwire measurements were carried out in the tab wake region and at several axial locations by means of a 99N10 DANTEC anemometry system using a Dantec 55P11 two-component probe. The hotwires were operated on a constant temperature with an overheat ratio of 1.5. The probe has platinum plated tungsten wires (1.25 mm long and 5 μm diameter) and can be used for air applications with turbulent intensities up to 5–10. The X-wire was positioned in the flow was such that it allowed to measure the fluctuations of streamwise velocity (u') and transverse velocity (v'). The positioning of the anemometer sensor was performed by using a PC-controlled precision positioning device. The probe was calibrated using Dantec 9054H01 calibrator with 120 mm^2 nozzle in the velocity range

between 0 and 25 m s^{t1}. The signals from the probe were acquired at a sampling rate of 3 kHz with 10,000 samples. The anemometer analog output was acquired by using a differential mode National Instruments PCI-6036E having 16-bit resolution, operating range of ± 10 V and maximum scan rate of 200 Ks/samples. The linearization and processing of the hotwire signal was then carried out digitally. The actual streamwise velocity U and the perpendicular velocity V were calculated from the hotwire anemometer output according to King's law equation and equation procedure by Jorgenson [29]. The uncertainty in the jet exit velocity U_e and the positioning of the hotwire X-probe is $\pm$ 0.5 m s^{-1} (2.5%) and $\pm$ 0.5 mm (2%), respectively. It may however be pointed out that the length of the sensor elements is relatively large as compared with the cylindrical tab dimensions, and the projected dimension of the sensor elements to the oncoming flow is 0.8 mm. Therefore, the uncertainty in measurements with regard to the probe dimensions is approximately 2%.

3. Results and discussions

3.1. *Jet centreline decay and half-width growth*

Figure 3(a) shows a comparison of the jet centreline velocity decay for the cases investigated using hotwire. It can be seen that the presence of cylindrical tabs enhances the overall jet mixing by bringing down the potential core length from $3.0D_e$ for a plain jet to approximately $1.84D_e$ ($h/d = 1.0$; 39% reduction) and $1.05D_e$ ($h/d = 1.67$; 65% reduction). Thereafter, a faster decay in the centreline velocity is also indicated for tabbed jets. When compared with a tab with flat front and back surfaces (square configuration with similar percentage of blockage area), the cylindrical tab shows similar potential core length but a slower jet decay thereafter. Cylindrical tabs are also seen to significantly increase the turbulent intensity along the jet centreline compared with plain jet, as shown in Figure 3(b). For the plain jet, the peak in turbulence intensity u'/U_e occurs for $X/D_e > 5.6$, whereas for the jet with tabs ($h/d = 1.0$) this location shifts upstream to $X/D_e = 5.3$. Increasing the tab height ($h/d = 1.67$) further improves the turbulent intensity and shifts the location of peak intensity to $X/D_e = 4.7$. Relative to the cylindrical tab, the flat tab is seen to contribute towards improved centreline turbulent intensity. The above trends show enhancement of both large-scale and small-scale activities for an elliptic jet with tabs and with increase in the tab height.

The effect of cylindrical tabs on jet growth in each plane can also be seen from the jet half-width plots, as shown in Figure 3(c). For the plain case, the jet is seen to grow along the minor-axis plane, while it shrinks along the major-axis plane (as is known). At $X/D_e = 4.6$, the jet half-width plots along the two planes are seen to cross each other, indicating the location of axis-switching. Tabs are seen to initially inhibit the jet growth in the minor-axis plane, but for $X/D_e > 4.0$ the jet growth becomes similar to that of the plain jet. However, in the major-axis plane, the jet spread increases significantly (because of jet-core bifurcation, discussed later), unlike the plain jet. As a result, axis-switching in the tabbed elliptic jet was not observed, as seen in Figure 3(c). Increasing the tab height further enhances the jet spread in the major-axis plane.

3.2. *Flow visualization*

It is well known that a plain elliptic jet grows dramatically along the minor-axis plane and shrinks along the major-axis plane, resulting in axis-switching at some downstream location, as shown in Figure 3(b). This is primarily caused by the non-uniform induction of velocity along the azimuthal direction [7]. Figures 4(a–d) show the raw PIV images of

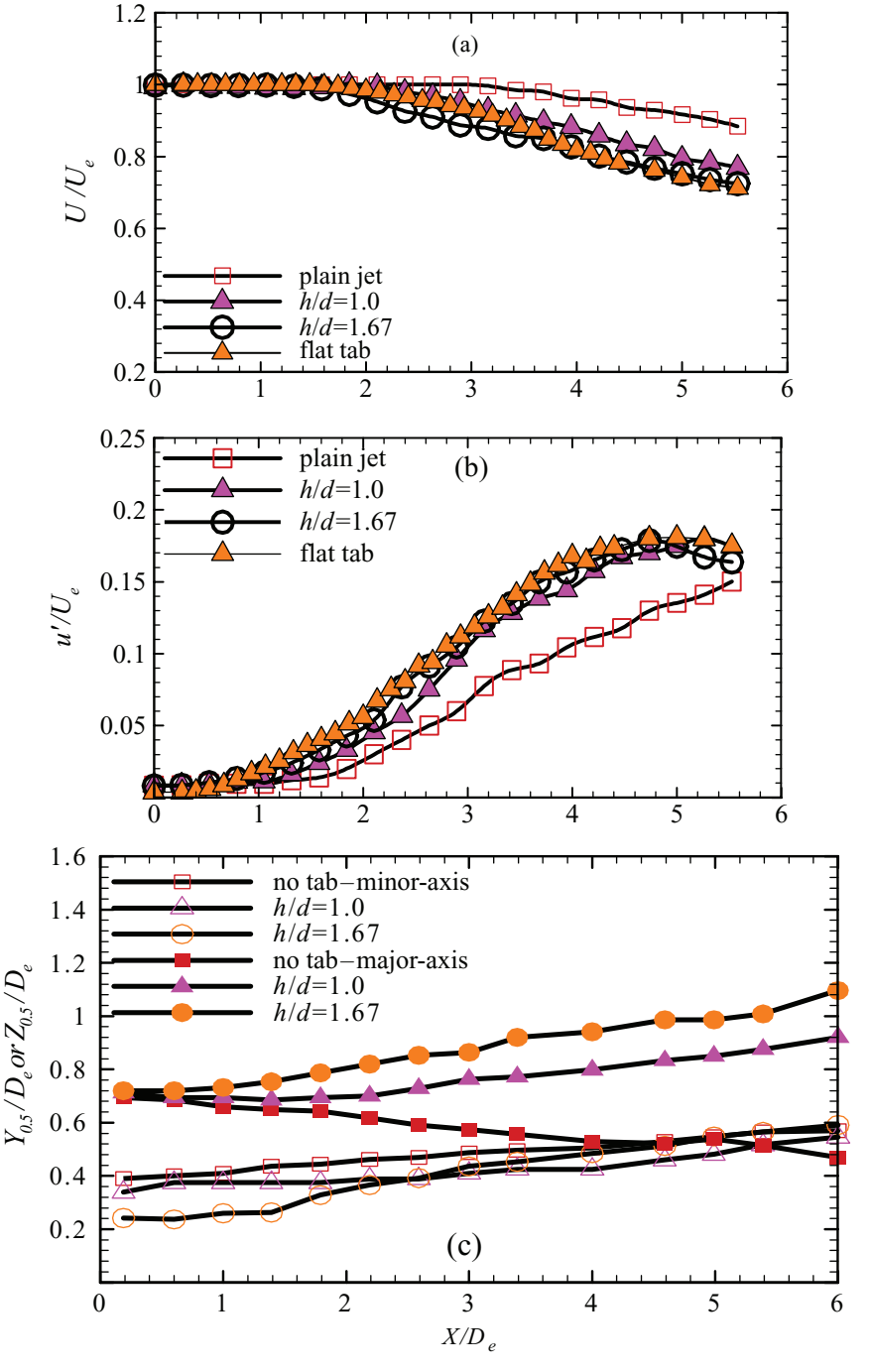

Figure 3. (a) Centreline velocity (U/U_e) decay for jets issuing from a 2:1 elliptic nozzle with and without tabs, (b) effect of tabs and tab height on the u'/U_e centreline distribution, and (c) jet half-width growth for plain and tabbed jets along the $X-Y$ and $X-Z$ planes.

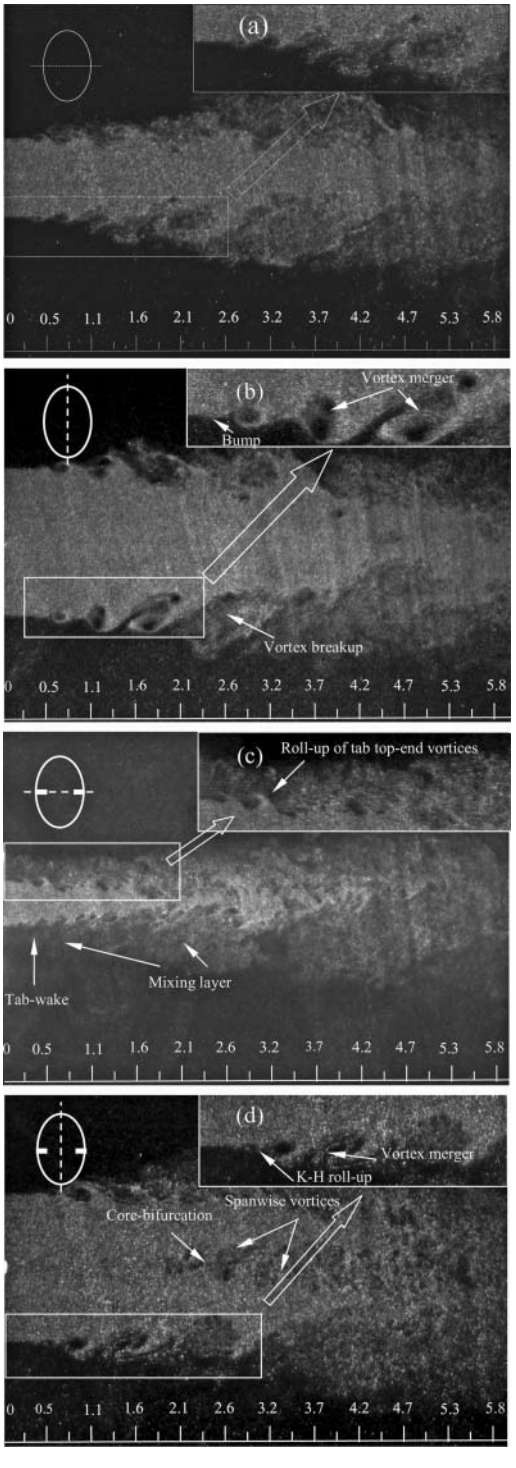

Figure 4. Raw PIV images of the jet showing flow development for a plain elliptic nozzle along (a) the minor-axis plane and (b) the major-axis plane; and for a tabbed elliptic nozzle along (c) the minor-axis plane and (d) the major-axis plane; $h/d = 1.67$ (scale in mm). (e) A schematic diagram of the streamline flow pattern around tabs of different configurations.

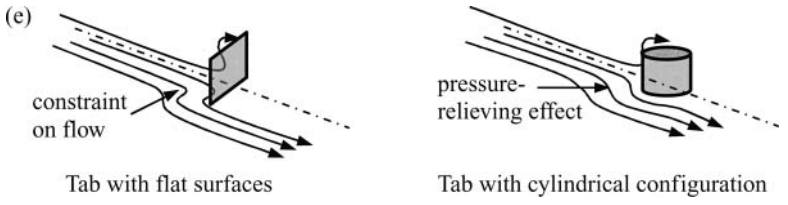

Figure 4. *(Continued)*

the jet flow development. A magnified portion of the region of interest is shown in the inset for each image to bring out the flow structure development in each case. For the plain jet, it can be seen that the jet begins to distort at $X/D_e = 0.44$, as shown in Figures 4(a–b), and is attributed to the Kelvin–Helmholtz (K-H) roll-up associated with the shape of the inflectional mean velocity profile [21]. Before the roll-up begins, a bump is seen at the edge which signals the beginning of the K-H wave instability, as shown in Figure 4(b). These waves amplify and eventually roll-up to form vortical structures that grow in size as they are convected downstream. The vortical structures appear to be the largest at $X/D_e = 1.3$, and tend to break up thereafter.

The placement of tabs along the minor-axis side dramatically modifies the jet development along both planes, as shown in Figures 4(c–d). The flow visualization image (Figure 4c) shows that the flow in the wake region of the cylindrical tab is not completely blocked but only partially (unlike thin tabs with flat front and back surfaces [15,21]), owing to the sideways pressure-relieving effect of a tab with cylindrical configuration (along its span due to circular curvature). This freedom of sideways movement relieves the constraint on the flow relative to a thin tab with flat surfaces, as shown in Figure 4(e), i.e. the flow does not have to speed up to that extent to flow past such a tab and so the changes in velocity and pressure are smaller [30]. Therefore, while passing a tab of cylindrical configuration the flowis more relaxed and somewhat relieved in comparison to the flow past thin tab with flat front and back surfaces, as shown in Figure 4(e). The presence of large quantities of seed particles in the tab wake region distinctly shows this important feature.

Along the minor-axis plane (Figure 4c), the flow emanating from the tab free-end is seen to roll-up into small-scale K-H vortices which gradually move towards the jet centreline as the flow is convected downstream. The major-axis plane of the jet, on the other hand, shows the appearance of a pair of vortices of opposite sense along the jet centreline at an approximate location that marks the end of the jet potential core (Figure 3a), and beginning location of jet-core bifurcation, as shown in Figure 4(d). Increasing the tab height is seen to further shift this location upstream (Figure 3a). As a result, the jet issuing from an elliptic nozzle with tabs grows considerably along the major-axis plane, while no significant change in the jet growth is seen along the minor-axis plane, as shown in Figure 3(c).

3.3. *Mean velocity characteristics and PIV measurements*

3.3.1. *Major-axis plane*

Figures 5(a–c) show contours of mean velocity (superimposed with total velocity vectors) for the plain and tabbed jets ($h/d = 1.0$ and 1.67), respectively, along the major-axis plane. Near top-hat mean–velocity vector profiles are seen for the plain jet close to the nozzle exit, indicating uniform seeding and good PIV measurements. However, in Figure 5(c), close to the nozzle exit an erroneous inflection point is seen that is caused by reflection of stray laser light on the tab (also seen in the raw PIV image, Fig 4d). Thereafter, near top-hat

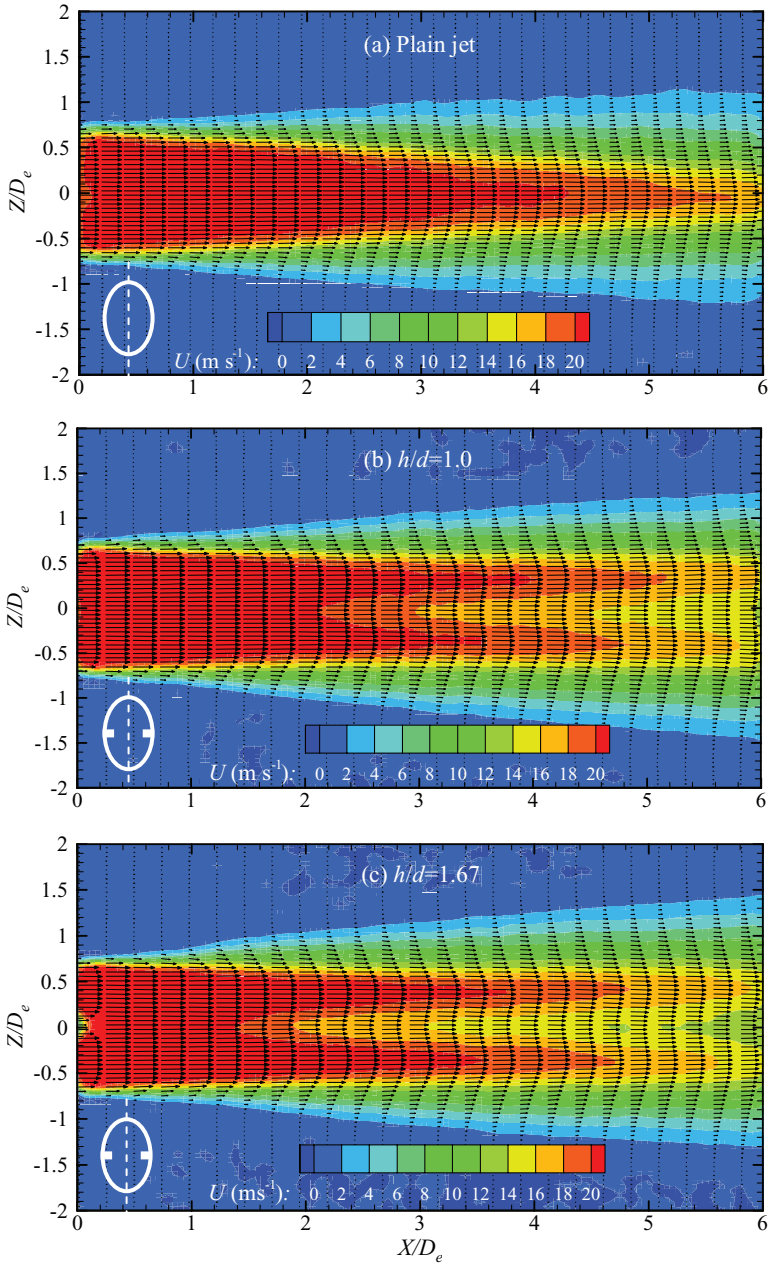

Figure 5. Mean velocity and vector plot showing jet development from a 2:1 plain elliptic jet in the major-axis plane: (a) plain jet, (b) with tabs ($h/d = 1.0$), (c) with tabs; $h/d = 1.67$.

profiles are observed until the location of jet-core bifurcation is reached. For $h/d = 1.0$, the beginning of jet-core bifurcation and inflection point are seen to occur at $X/D_e = 2.0$, as shown in Figure 5(b). This axial location is seen to shift upstream with increase in tab height (Figure 5c), which also corresponds to the axial extent of the jet potential core, as seen in Figure 3(a).

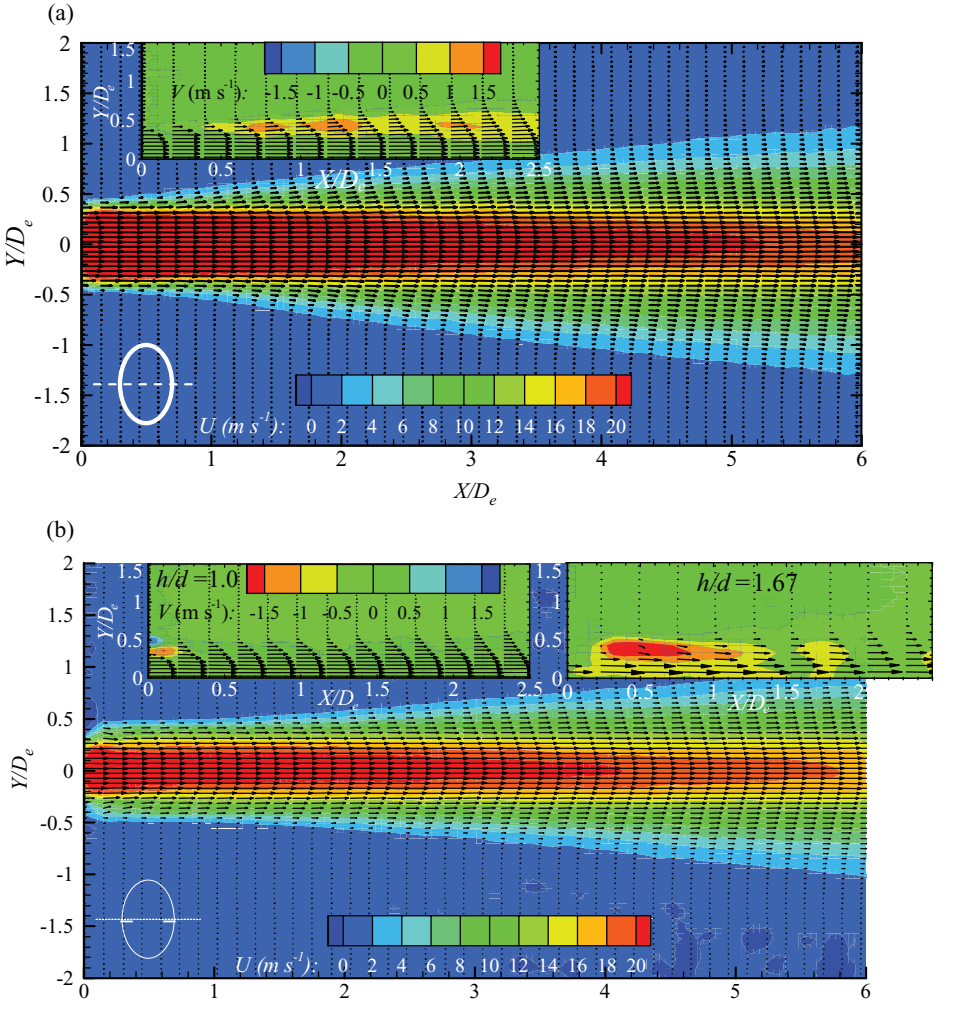

Figure 6. Mean velocity and vector plot showing jet development from a 2:1 elliptic jet in the minor-axis plane: (a) plain jet and (b) with tabs; h/d = 1.0 and h/d = 1.67.

3.3.2. *Minor-axis plane*

Figures 6(a, b) show the mean axial velocity contours (superimposed with total velocity vectors) for plain and tabbed ($h/d = 1.0$) jets, respectively, in the minor-axis ($Y - Z$) plane. For the plain jet, a region of positive V is seen to develop as the shear-layer grows downstream, as shown in the inset of Figure 6(a). The placement of tabs modifies the flow development significantly. Immediately downstream of tabs, a small region of low axial mean velocity exists. The two insets in Figure 6(b) are a zoom of the flow process and show contours of mean V-component for the two tab heights. It is seen that cylindrical tabs produce a region of the strong positive mean V-component immediately behind the tab, the axial and vertical extent of which increases with increase in the tab height. This completely alters the shear-layer growth in this plane as compared with the plain jet. For the smaller tab, this region gets dispersed faster and shows the appearance of the positive

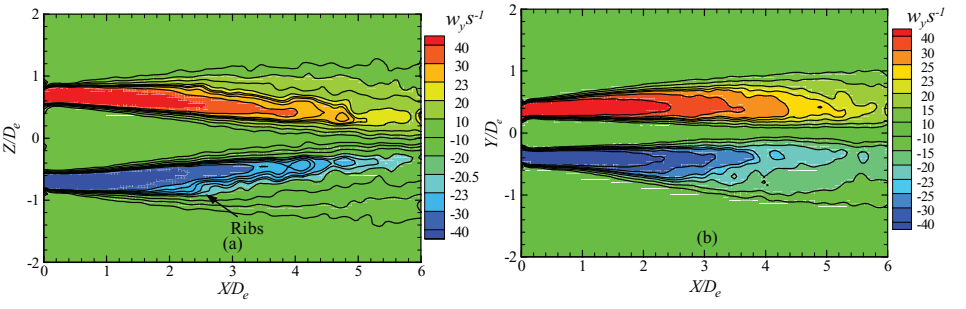

Figure 7. Time-averaged vorticity maps captured for the plain elliptic jet: (a) major-axis plane and (b) minor-axis plane.

V-component much earlier. However, the negative V-component for $h/d = 1.67$ is seen to persist further downstream.

3.3.3. *Averaged and instantaneous vorticity maps*

Figure 7 shows the time-averaged vorticity maps for the plain elliptic jet along its minor- and major-axis planes. Mean flow features show the presence of 'ribs' in the jet shear-layer along the major-axis plane (Figure 7a), while no such feature can be seen clearly along the minor-axis plane, as shown in Figure 7(b). These ribs are associated with the longitudinal vortical substructures [31–32] or the streamwise-oriented vortices in mixing shear-layers and are formed as a result of the vortex roll-up and vortex-stretching mechanisms. This occurs approximately downstream of the vortex merger seen in Figure 4(b). The formation of a small indentation in the contours or a 'valley' [33] adjacent to the rib can also be discerned, indicating the movement of vortex roll-ups towards the jet centreline, thereby initiating the process of mass entrainment and mixing in shear layers. The formation of ribs can also be seen along the major-axis plane of the jet with tabs, as shown in Figure 8(a). Additionally, a trail of oppositely signed vortices (spanwise vortices discussed later) appears at the jet centreline at approximately $X/D_e = 1.2$, causing bifurcation of the jet core. Behind the tab, two regions of like-signed vorticity can be observed, suggesting the development of flow structures from the free-end and base regions of the tab, as shown in Figure 8(b).

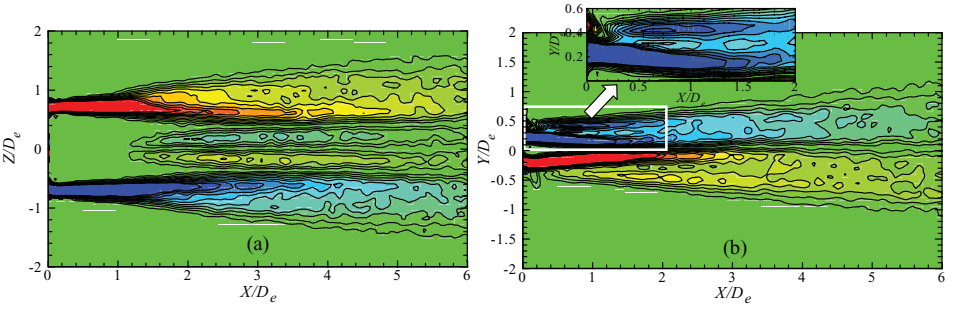

Figure 8. Time-averaged vorticity maps captured for the elliptic jet with tabs ($h/d = 1.67$): (a) major-axis plane and (b) minor-axis plane.

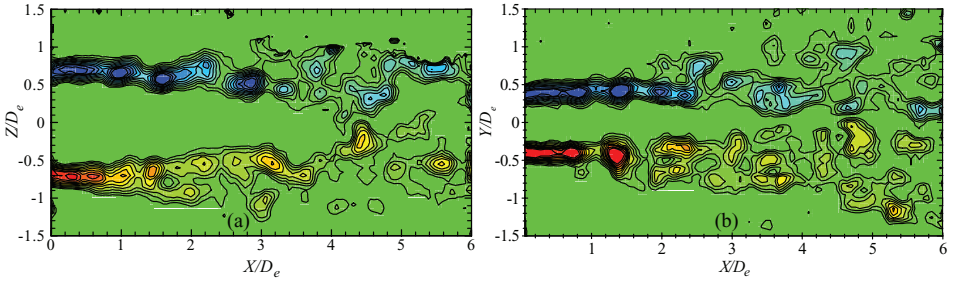

Figure 9. Instantaneous vorticity maps captured for the plain elliptic jet: (a) major-axis plane and (b) minor-axis plane.

The instantaneous vorticity maps are in good agreement with the mean flow features observed so far and those observed from raw PIV images. These maps clearly show the vortex roll-up, merger and rib structure formation (Figure 9a) along the major-axis plane for the plain case. The presence of tabs clearly shows the vortex roll-up from the free-end and base regions of the tab that cause significant mutual interactions between the flow structures and their breakdown (Figure 10b). Along the major-axis plane, a pair of oppositely signed vortices can be seen along the jet centreline which are being shed alternately (Figure 10a). The evidence gathered so far suggests that two vortical structures are shed from the cylindrical tab: one close to the tab base region and the other one from the tab free-end. As these wake structures move downstream towards the jet centreline, they entrain fluid and coalesce, thereby growing in extent.

3.4. *Hotwire measurements*

The state of the jet exit shear layer where the cylindrical tabs are placed was turbulent and the Reynolds number based on the tab diameter, $Re_d = 4263$. At this Reynolds number, alternate shedding of spanwise vortices is known to occur behind a circular cylinder. Furthermore, the jet exit shear-layer thickness ($U = 0.99U_e$) along the minor-axis side, δ_{mi}, was about 1.25 mm or $0.42d$ at the tab axis and that along the major-axis side of the nozzle, δ_{mj}, was about 1.75 mm, respectively. Therefore, the tabs with $h/d = 1.0$ and 1.67 protrude into the flow. The corresponding displacement thickness along each nozzle axis is

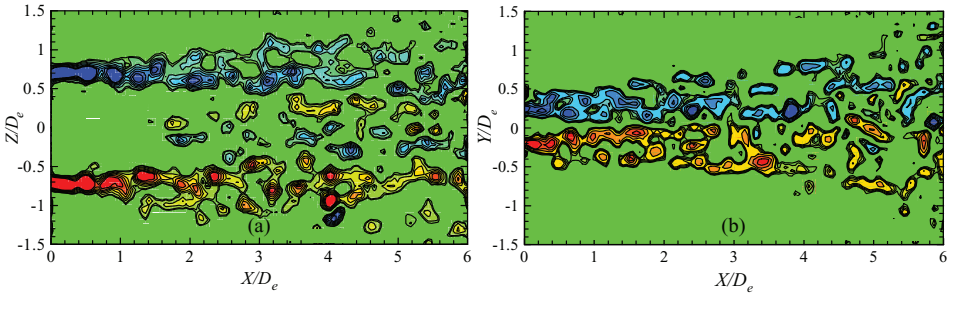

Figure 10. Instantaneous vorticity maps captured for the elliptic jet with tabs ($h/d = 1.67$): (a) major-axis plane and (b) minor-axis plane.

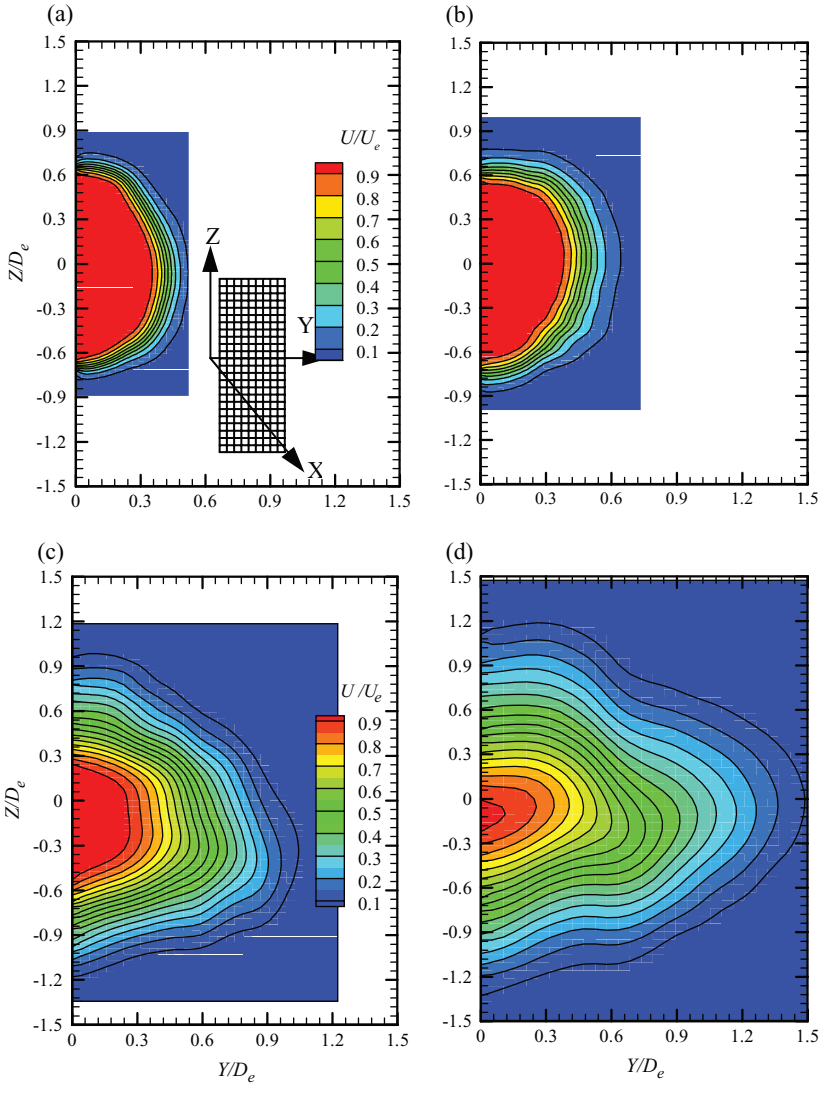

Figure 11. Contours of mean velocity for a plain elliptic jet at different axial locations in the $Y - Z$ plane: (a) $X/D_e = 0.5$, (b) $X/D_e = 1.0$, (c) $X/D_e = 3.0$ and (d) $X/D_e = 5.0$.

$0.127d$ and $0.178d$, respectively. The jet flow longitudinal turbulence ($u^{'}/U_e$) at the nozzle exit was about 0.3% at 20 m s^{t1}.

3.4.1. *Overall jet development*

Mean velocity distribution contours. Figure 11 shows the contours of normalized streamwise mean velocity (U/U_e) for the plain jet at four axial locations of $X/D_e = 0.5$, 1.0, 3.0 and 5.0, respectively. Extensive grid measurements were made in one-half $Y - Z$ plane of the jet (as shown in Figure 1b) with a step size of $\Delta y = \Delta z = 1.0 \pm 0.1$ mm or $0.026D_e$ for $X/D_e = 0.5$, 1.0 (approx. 1600 and 2400 points, respectively) while a step

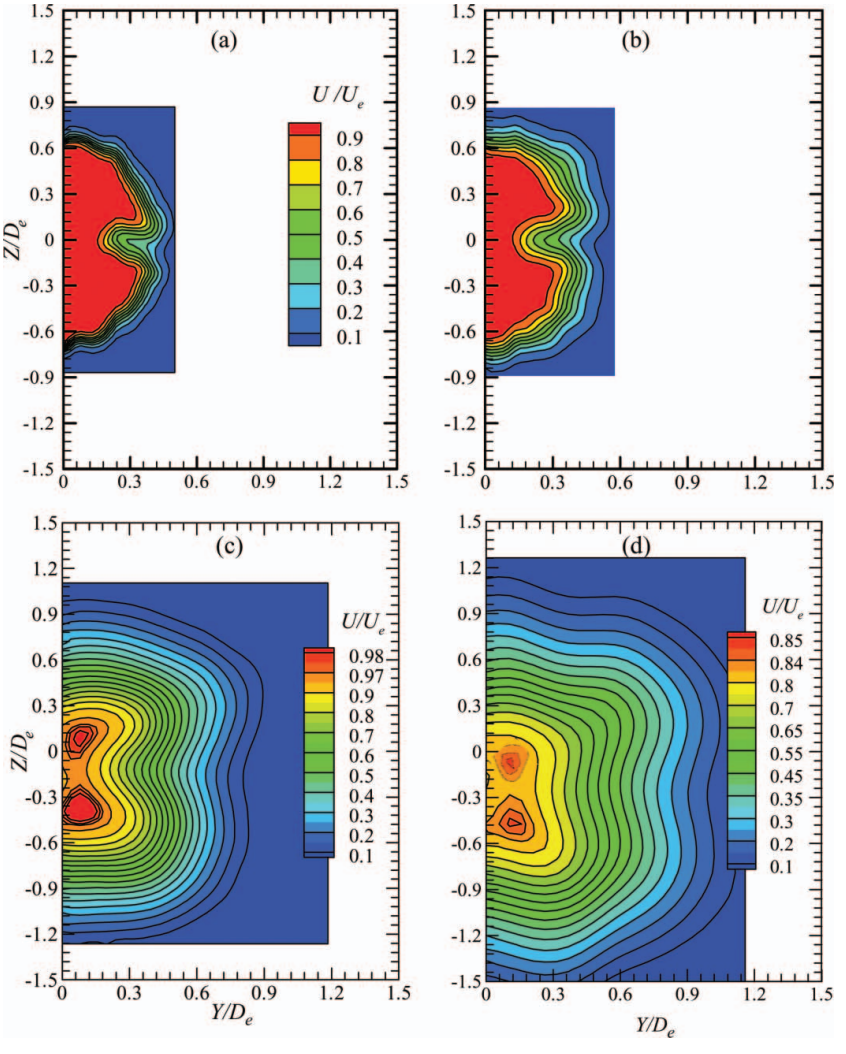

Figure 12. Contours of mean velocity for an elliptic jet with tabs ($h/d = 1.67$) at different axial locations in the $Y - Z$ plane: (a) $X/D_e = 0.5$, (b) $X/D_e = 1.0$, (c) $X/D_e = 3.0$ and (d) $X/D_e = 5.0$.

size of $\Delta y = \Delta z = 1.5 \pm 0.1$ mm or $0.039D_e$ was kept for $X/D_e = 3.0$, 5.0 (approx. 1250 and 1600 points, respectively). The variation in each successive contour level is $0.1U_e$ for Figures 12(a–b) while in Figures 12(c–d) it is $0.05U_e$.

Immediately downstream of the nozzle exit, the jet retains its original elliptic shape of the nozzle and shows a thin mixing layer (Figure 11a). As the jet begins to deform due to non-uniform induction of the velocity along the azimuthal direction [7], mixing between the jet and the ambient irrotational mass is initiated, wherein the ambient irrotational mass is brought in towards the jet centreline along the major-axis side and the jet mass is thrown out along the minor-axis side. Further downstream, the mixing layer begins to thicken and the jet cross-section begins to change shape with faster jet growth along the minor-axis side, as seen in Figure 11(c). At $X/D_e = 3.0$, the jet cross-section takes a near-circular shape. Further downstream at $X/D_e = 5.0$, the jet shape again becomes elliptic, but this time with

its minor-axis along the Z-direction and major-axis along the Y-direction, respectively. The plain jet therefore switches axis at $X/D_e = 4.5$ (as also seen in Figure 3b).

The introduction of tabs in the minor-axis side significantly modifies the overall jet development characteristics, as shown in Figure 12. In the region immediately behind the tab, there is an indentation in the jet core which is a region of low-speed fluid and bifurcates the jet into a two 'finger' structure, as shown in Figures 12(a–b). The inward penetration of the wake inhibits jet growth along the minor-axis plane, and a lateral increase in the wake width helps promote jet growth along the major-axis plane. This prevents the jet to switch axis, a flow characteristic completely reverse of that observed for a plain elliptic jet (Figure 11). The velocity deficit caused by the tabs is also seen to disappear by $X/D_e = 5.0$, as shown in Figure 12(d), while the jet-core bifurcation is clearly seen to occur at $X/D_e =$ 3.0 and 5.0.

3.4.2. *Tab wake region*

Profiles of mean velocity, turbulence intensity and Reynolds shear stress. The wake of a finite-length cylinder mounted on a flat plate has been studied extensively primarily due to the high degree of three-dimensionality introduced by the free-end and the wall boundary-layer making its wake characteristics very different from that of a two-dimensional cylinder [34]. This type of flow is now known to be characterized by the presence of three major components, namely the downwash flow from the free-end of the cylinder, the spanwise shear flow [26] and the upwash from the base of the cylinder. Earlier studies [24, 35, 36] have shown that the nature of base vortex (especially its size) depends primarily on the boundary-layer conditions, i.e. it is practically found to be absent when δ is negligibly thin. As a result, the cylinder h/dsignificantly affects the flow structure development. For the present study, detailed hotwire measurements were made (i) along the tab axis and (ii) perpendicular to the tab axis (step size of 0.25 $\pm$ 0.1 mm) to investigate the type of flow structures being shed in the near-wake region of the tab.

Along the tab axis. Figures 13(a–c) show the mean velocity (U/U_e), turbulence intensity (u'/U_e) profiles and Reynolds shear stress ($u'v'/U_e^2$) profiles measured at various

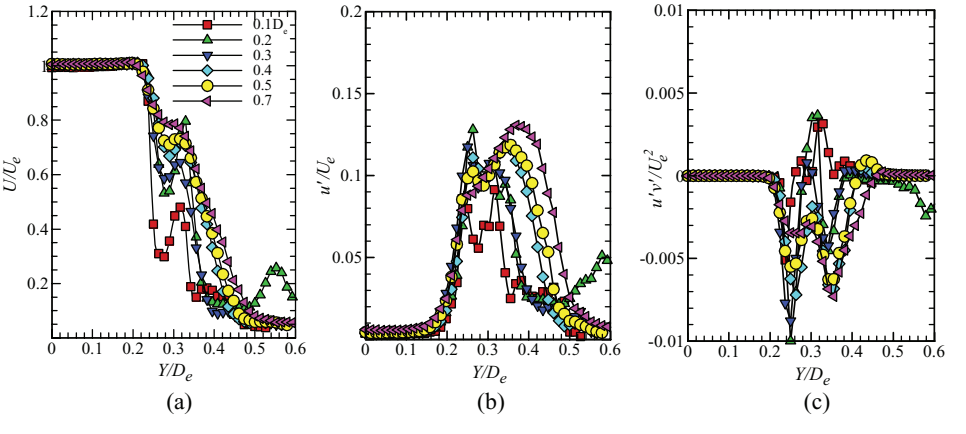

Figure 13. Profiles measured at various streamwise locations along the tab axis ($Z = 0$) for (a) mean velocity (U/U_e), (b) turbulence intensity (u'/U_e) and (c) Reynolds shear stress ($u'v'/U_e^2$).

streamwise locations along the tab axis ($Z = 0$), respectively. The mean velocity profiles at $X/D_e = 0.1$, 0.2 and 0.3 reveal two distinct regions of velocity minimum and maximum, as seen in Figure 13(a). Near the region of the tab base (at $Y/D_e = 0.32$) a maximum in U/U_e occurs followed by a minimum between the tab mid-height and free-end. These correspond to the upwash from the base vortex and the downwash from the tab free-end, respectively. As the tab free-end is approached, the U/U_e value sharply increases to its value in the jet core, causing a shear layer to develop that gradually begins to roll-up into small-scale K-H vortices. The corresponding turbulent intensity (u'/U_e) profiles (Figure 13b) show intense mixing near the base and free-end regions of the tab. The Reynolds stress distribution also shows an inflection point at the location of the velocity deficit, suggesting independent flow structure development from the base and free-end regions of the tab, as seen in Figure 13(c). With increasing streamwise distance from the tab, the strong velocity deficit at tab mid-span reduces (due to vortex interaction and viscous diffusion) and is seen to move inwards the jet core between $X/D_e = 0.5$ and 0.7. As the wake structures move into the jet core, they entrain the jet/ambient fluid into the wake and coalesce, thereby causing the wake region to spread more uniformly with the high-speed jet core fluid.

Perpendicular to tab axis. Measurements were also made perpendicular to the tab axis at $Y/D_e = 0.355$, 0.289 and 0.25 at $X/D_e = 0.10$, 0.15, 0.20 and 0.40. Each of these Y/D_e locations corresponds to the region of the tab base, 0.5 mm below the tab free-end and 1 mm above the tab free-end, respectively. Figures 14(a–c) show the mean velocity (U/U_e), turbulence intensity (u'/U_e) and Reynolds shear stress ($u'v'/U_e^2$) profiles obtained in the region of the tab base or at $Y/D_e = 0.355$. The U/U_e plots in Figure 14(a) show 'W-shaped' profiles with two minima and three maxima. Each of these minima is flanked by a maximum which indicates strong cross-stream gradients on each side of the tab axis and is responsible for the generation of a base vortex with its axis aligned along the streamwise direction. The appreciable increase in U/U_e at the tab axis signifies a strong upwash resulting from the flow ejection by a base vortex system shed behind the tab. Since δ for the present case is $0.4h/d$, a large base vortex shed behind the tab entrains the high-speed fluid from the jet core towards the tab base and into its wake. Further downstream, this upwash shows a drop in value and almost disappears at $X/D_e = 0.40$. This is unlike the case for a wall mounted cylinder which shows a strong velocity deficit at the tab axis (in the base region) that manifests the upward motion of low-speed fluid from the surface which decays rapidly [37]. The flow development however gets modified when the cylindrical tab is placed at the exit of an elliptic nozzle which has a non-uniform azimuthal curvature variation. The base vortices shed from the tab create an 'engulfing-effect' wherein the ambient fluid is brought inwards into the jet core flow while the jet core fluid is ejected in a direction perpendicular to the tab axis and towards the major-axis. This large perturbation introduced by the tabs in the azimuth of the elliptic nozzle interferes with the azimuthal instability process of the elliptic jet, thereby significantly modifying the process of azimuthal distortions. Furthermore, the interaction between the base vortices and the spanwise vortices produced by the K-H instability causes the spanwise vortices to stretch out and hence introduce intense small-scale turbulence which enhances mixing of jet flow with the ambient flow [38]. The presence of a pair of base vortices therefore modifies the process of azimuthal distortion in such a way that it inhibits jet growth along the minor-axis side, while promoting growth in major-axis side. The base vortices introduce intense mixing in the wake region with the highest u'/U_e intensity seen along the region of flow ejection (i.e. along the tab axis) and near the tab sides, as shown in Figure 14(b). With increasing distance from the

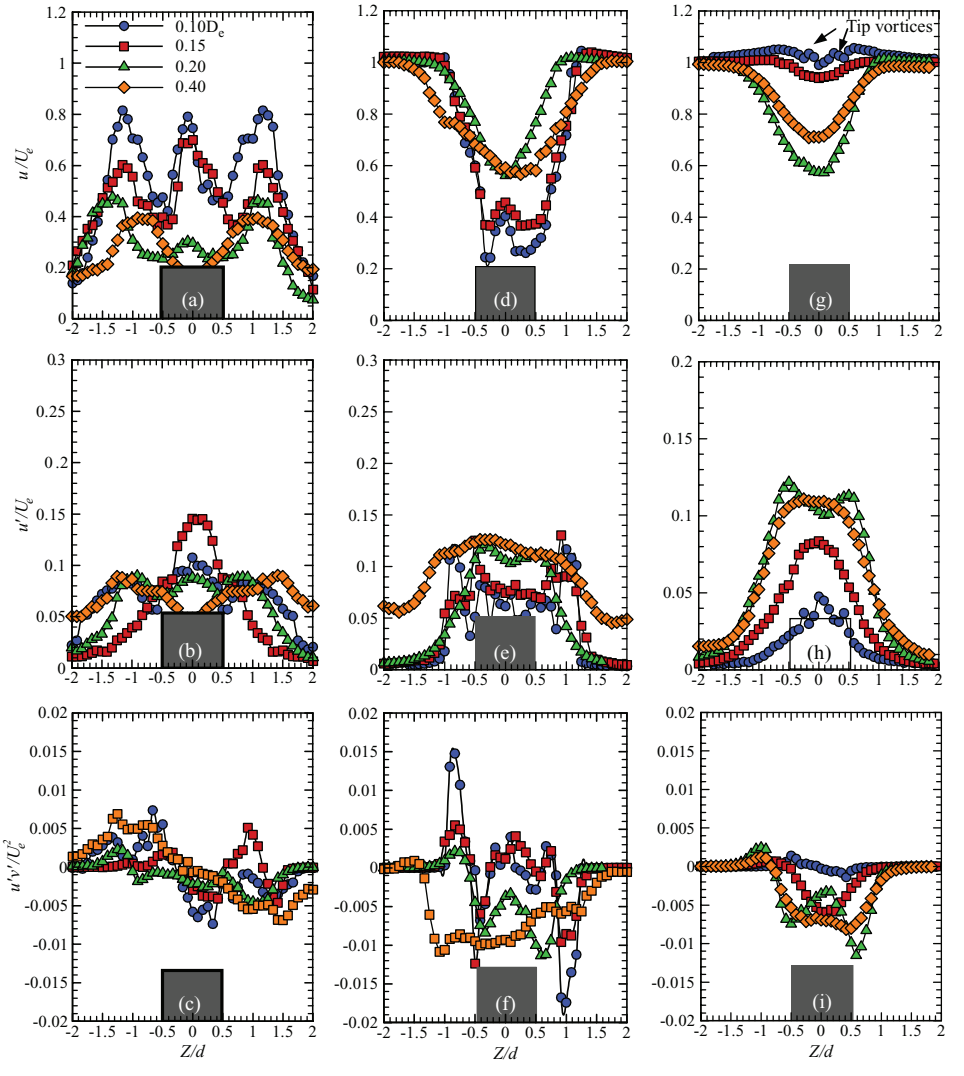

Figure 14. Profiles of mean velocity (U/U_e), turbulence intensity (u'/U_e) and Reynolds shear stress ($u'v'/U_e^2$) measured perpendicular to the tab axis in the region of (a–c) the tab base, $Y/D_e = 0.355$, (d–f) tab free-end, $Y/D_e = 0.289$, and (g–i) 1.0 mm above tab free-end, $Y/D_e = 0.25$.

tab, a rapid lateral growth of initially generated vortical structures and mass–momentum exchange occurs, which stimulates intense mixing.

Figures 14(d–f) show the corresponding profiles obtained from measurements made 0.5 mm below the tab free-end or at $Y/D_e = 0.289$. Once again, the U/U_e profiles show a W-shape but with a peak in U/U_e near the tab axis of a much less value as compared with that seen near the tab base, as shown in Figure 14(a). This increase in the U/U_e value near the tab free-end is apparently due to the downwash flow which brings in high-speed fluid from the jet core into the tab wake. The peak however disappears as the flow is convected downstream, where only a velocity deficit can be seen at $X/D_e = 0.20$ and 0.40, suggesting the end of the upper limit of the downwash flow from the tab free-end behind the tab. Thin

shear layers (seen as sharp velocity gradients on the edges of the tab) are seen to develop from the edges of the tab (Figure 14f), which gradually grow due to lateral diffusion and form the spanwise vortices. The spanwise separating shear layers coalesce rapidly, which facilitates growth in its scale, while the strong upwash from the base vortices (as they are convected downstream) results in a vertical penetration of the tab wake into the jet core and towards the jet centreline. These spanwise vortices (from each tab) later on make themselves appear at some downstream distance along the centreline, as seen in raw PIV images, mean and instantaneous vorticity plots in Figures 4(d), 6(b) and 8(b), respectively. This location also marks the beginning of the jet-core bifurcation. The interaction between the downwash from the free-end and the spanwise shear flow makes the near wake of the tab highly three-dimensional, thereby introducing intense local mixing, as shown in Figure 14(e).

For measurements 1 mm above the tab free-end or at $Y/D_e = 0.25$ (Figures 14g–i), the U/U_e plot at $X/D_e = 0.10$ shows an 'M-shaped' profile (instead of the W-shaped profiles observed so far) with a velocity deficit at the tab axis which is flanked by peaks on either side that are well within the lateral dimensions of the tab free-end. The peak pattern on either side of the tab axis suggests the presence of small-scale tip vortices with their sense of rotation opposite to that of the large base vortices. Further downstream at $X/D_e = 0.15$, these peaks disappear and the profiles show only a velocity deficit at the tab axis which increases with increasing X/D_e. This indicates that the flow from the tab free-end initially moves upwards and then downwards along with the downwash flow from the tab free-end, resulting in the generation of tip vortices [34–36]. Significant mixing is introduced in this region, as seen in Figure 14(h), resulting in lateral diffusion of the spanwise shear layers, as shown in Figure 14(i).

Mean velocity distribution contours. Figure 15 shows the contours of the normalized streamwise mean velocity (U/U_e) in the tab wake region acquired at three streamwise locations $X/d = 2.0$, 3.0 and 3.0, respectively. These contours are obtained from grid measurements on both sides of the tab in the $Y - Z$ plane (with $\Delta y = \Delta z = 0.5 \pm 0.1$ mm or $0.013D_e$ and resulting in 1073 points), as shown in Figure 1(c). Such detailed measurement grids were required because of the highly three-dimensional evolution of the flow behind the tab. The innermost contour line indicates the approximate edge of the boundary layer (where $U/U_e = 0.95$); Figures 15(a, c, e). The variation in each successive contour level is $0.1U_e$ for Figure 15(a), while in Figures 15(c, e) it is $0.05U_e$. Initially, the air is seen to wrap around the tab (Figure 15a) and develop into a 'mushroom structure' immediately behind the tab (Figures 15c, e). The mean velocity is seen to decrease sharply as the tab wake region is approached, decreasing approximately to $0.3U_e$, indicating strong cross-stream gradients. Near the tab base region, a sharp incursion of contours is observed on each side, which suggests the presence of a streamwise vortex (of clockwise rotation on the right side and vice versa as shown by arrows), as seen in Figure 15(c). This vortex system causes induction of high-speed fluid (from jet core) towards the tab base region and inwards along the tab axis, thereby promoting fluid and momentum exchange, and hence stimulating intense local mixing. With increasing distance from the tab, the thickness of the mixing layer increases (as expected) due to momentum exchange and dispersion of initial flow structures, both along the tab axis and along the axis normal to the tab placement, causing the mushroom structure to grow in size, as seen in Figure 15(e).

Figures 15(b, d, f) show the corresponding distribution of turbulence intensity in the tab wake region. The plots suggest that the turbulent intensity is the highest in the core of the base vortex where the local velocity is the lowest (Figures 15c, d) and is gradually seen to creep in towards the spanwise region, developing shear layer in Figure 15(f). The

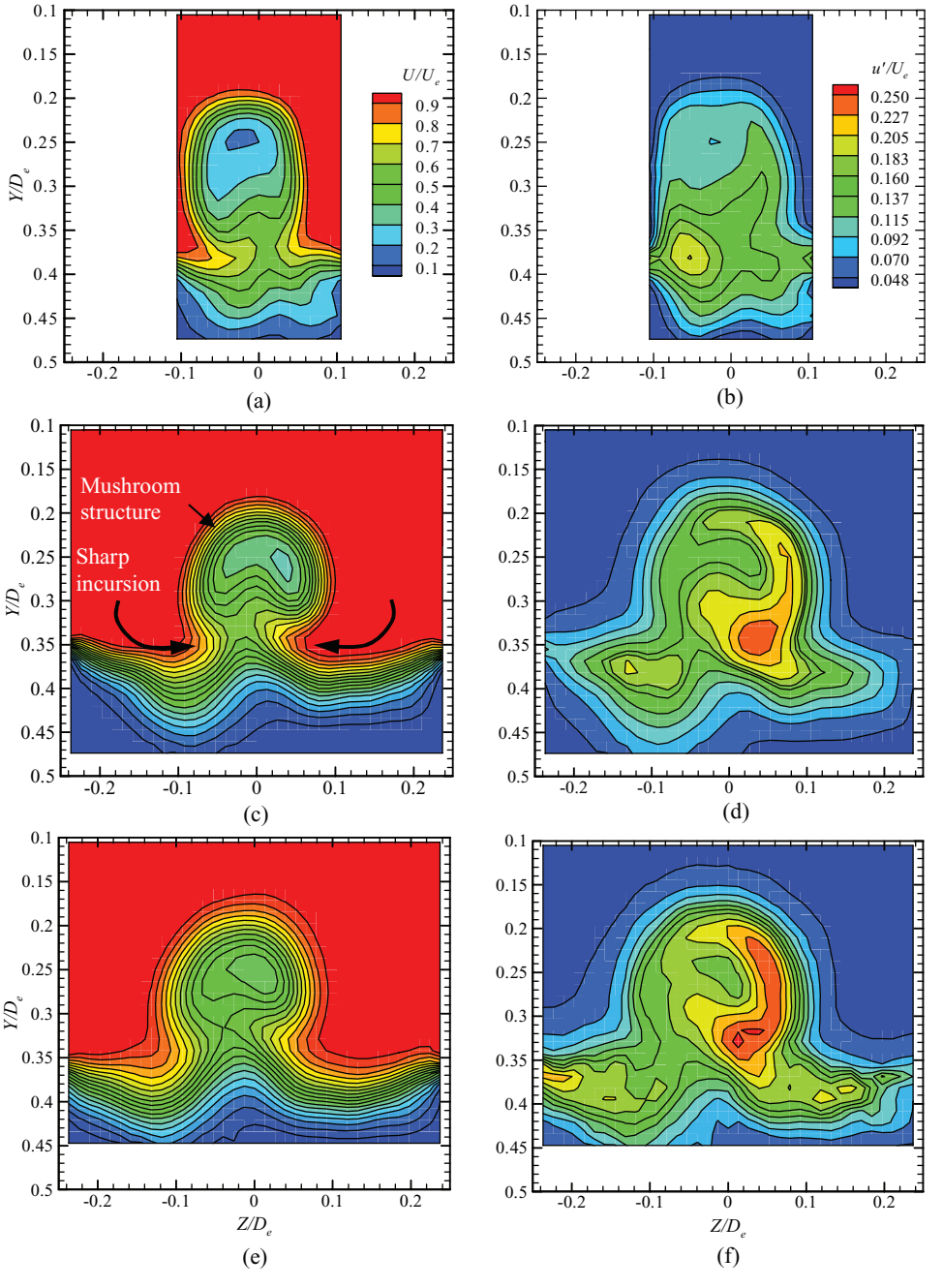

Figure 15. Contours of mean velocity and streamwise turbulence behind the tab ($h/d = 1.67$) at different axial locations in the $Y - Z$ plane; mean velocity (a–b) $X/d = 2.0$, (c–d) $X/d = 3.0$ and (e–f) $X/d = 4.0$.

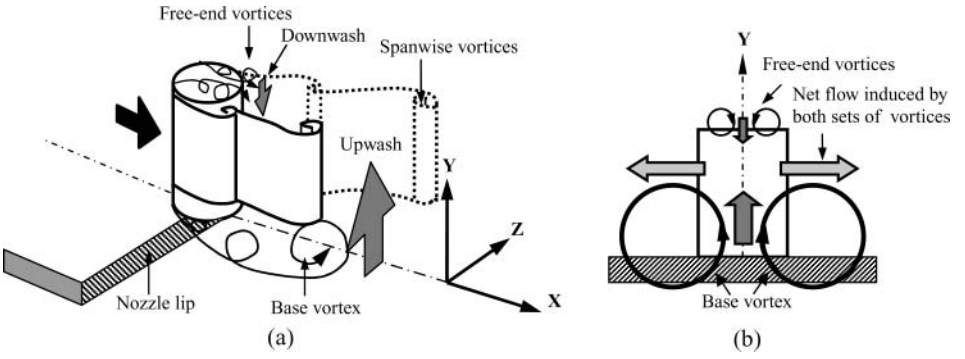

Figure 16. A schematic diagram of the flow structure development around a tab of cylindrical configuration placed in a jet flow at the nozzle exit.

upwash region at the tab base shows higher turbulence levels (25%) than those prevalent in the downwash region (5–10%) near the tab fee-end. The above evidence suggests that the vorticity in both the streamwise base vortex core and the spanwise-generated vortex contributes significantly towards the overall mixing.

3.5. *Flow structure model*

Figure 16(a) shows a schematic diagram of the flow structure development behind a tab of cylindrical configuration placed in a jet flow at the nozzle exit. Unlike thin tabs with flat front and back surfaces, the flow, while passing the tab of cylindrical configuration, is not completely blocked but only partially, as shown in Figure 4(e). This is attributed to the sideways pressure-relieving effect that relieves the constraint on the flow relative to thin tabs with flat surfaces. The flow, therefore, while passing a tab of cylindrical configuration is more relaxed and somewhat 'relieved' and so the changes in velocity and pressure are smaller.

The vortex dynamics behind a tab is initiated by the pressure differential between the upstream and downstream surfaces that causes the air to wrap around the edges of the cylindrical tab. Since δ for the present case is $0.4h/d$, a large base vortex system is generated behind the tab with its axis aligned along the streamwise direction. The sense of rotation of the base vortex system is such that it entrains the high-speed fluid from the jet core towards the tab base and inwards along the tab axis, resulting in a strong upwash, as shown in Figure 16(a). On the other hand, the flow from the tab free-end initially moves upwards and then downwards along with the downwash flow from the tab free-end, resulting in the generation of small-scale tip vortices with their sense of rotation opposite to that of the large base vortices. Additionally, thin shear layers develop from the edges of the tab along its vertical span that grow gradually due to lateral diffusion and form the spanwise vortices. The wake, therefore, mainly comprises of base vortices and tip vortices that are enveloped from the sides by spanwise vortical structures. This large perturbation introduced by the tabs in the azimuth of the elliptic nozzle interferes with the azimuthal instability process of the elliptic jet, thereby significantly modifying the process of azimuthal distortions. While the strong upwash from the base vortices causes an inward penetration of the wake inhibiting the jet growth along the minor-axis plane, the net flow induced by the vortices shed from the tab free-end and the base region tends to increase the lateral distance between

the oppositely signed spanwise vortices (Figure 16b) and hence increases the wake width that helps promote jet growth along the major-axis plane. The combined effect of the above also results in a rapid inward and lateral growth of spanwise generated vortices that later show at some downstream distance along the jet centreline which marks the end of the jet potential core and the beginning location of jet-core bifurcation.

4. Conclusions

An experimental investigation has been carried out on jets issuing from a 2:1 elliptic nozzle with mixing tabs. The study on jets with tabs of cylindrical configuration has not been reported before and was the main objective of this study. Unlike thin tabs with flat front and back surfaces, while passing such a tab configuration the flow is not completely blocked but only partially owing to the sideways pressure-relieving effect that relieves the constraint on the flow relative to thin tabs with flat surfaces. As a result, such a tab configuration can have important implications on the tab drag reduction when compared with a tab with flat front and back surfaces. Measurements were made for a jet exit velocity of 20 m s^{-1} and for Reynolds number based on the nozzle equivalent diameter (D_e) of 54,000. Furthermore, the effect of tab height ($h/d = 1.0$ and 1.67) was also investigated.

The presence of cylindrical tabs is seen to enhance the overall jet mixing by bringing down the potential-core length from $3.0D_e$ for plain jet to approximately $1.84D_e$ (for $h/d = 1.0$; 39% reduction) and $1.05D_e$ (for $h/d = 1.67$; 65% reduction). This mixing characteristic is similar to that of tabs with flat front and back surfaces. The jet decay thereafter is faster for the conventional flat tab. A detailed grid study in the wake region shows the evolution of a mushroom structure behind each tab that entrains the high-speed fluid from the jet-core towards the tab base and inwards along the tab axis, resulting in a strong upwash. The wake region mainly comprises of base vortices and tip vortices (shed from the tab free-end) that are enveloped from the sides by spanwise vortical structures. While the strong upwash from the base vortices causes an inward penetration of the wake inhibiting the jet growth along the minor-axis plane, the net flow induced by the vortices shed from the tab free-end and the base region tends to increase the lateral distance between the oppositely signed spanwise vortices and hence increase the wake width that helps promote jet growth along the major-axis plane. This simultaneously results in a rapid inward and lateral growth of spanwise generated vortices that later show at some downstream distance along the jet centreline which marks the end of the jet potential core and the beginning location of jet-core bifurcation. Increasing the tab height shifts this location further upstream and promotes still higher jet growth along the major-axis plane. As a result, axis-switching in tabbed elliptic jet was not observed.

Tabs with cylindrical configuration also help improve the centreline turbulent intensity by shifting the location of its peak intensity upstream. Relative to the plain jet, these trends indicate enhancement of both large-scale and small-scale activities with mixing tabs and with increase in the tab height. The interaction between the downwash from the free-end and the spanwise shear flow makes the near wake of the tab highly three-dimensional, thereby introducing intense local mixing. The upwash at the tab base and the spanwise shear layer flow region shows higher turbulence levels (25%) than those prevalent in the downwash region (5–10%) near the tab fee-end. This suggests that the vorticity in the streamwise base vortex core and that in the spanwise generated vortex causes a rapid increase in the wake width and a subsequent increase in the overall turbulent intensity.

References

[1] E. Gutmark, K.C. Schadow, S. Koshigoe, and K.J. Wilson, *Combustion related shear flow dynamics in elliptic jets*, AIAA J. 27(10) (1989), pp. 1347–1353.

[2] E. Gutmark, K.C. Schadow, and K.J. Wilson, *Subsonic and supersonic combustion related non-circular injectors*, J. Propul. Power 7(2) (1991), pp. 240–249.

[3] W.R. Quinn, *Experimental and numerical study of a turbulent free square jet*, Phys. Fluids 31(5) (1988), pp. 1017–1025.

[4] A. Krothapalli, D. Bagdanoff, and K. Karamcheti, *On the mixing of a rectangular jet*, J. Fluid Mech. 107 (1981), pp. 201–220.

[5] G.F. Marsters, *Spanwise velocity distributions in jets from rectangular slots*, AIAA J. 19(2) (1981), pp. 148–152.

[6] C.M. Ho and E. Gutmark, *Vortex induction and mass entrainment in a small-aspect-ratio jet*, J. Fluid Mech. 179 (1987), pp. 383–405.

[7] F. Hussain and H.S. Husain, *Elliptic jets, Part 1: Characteristic of unexcited and excited jets*, J. Fluid Mech. 208 (1989), pp. 257–320.

[8] W.R. Quinn, *On mixing in an elliptic turbulent free jet*, Phys. Fluids 1(10) (1989), pp. 1716–1722.

[9] S.B. Verma and E. Rathakrishnan, *Flow and acoustic properties of underexpanded elliptic-slot jets*, AIAA J. Propul. Power 17(1) (2001), pp. 47–57.

[10] D.G. Crighton, *Instability of an elliptic jet*, J. Fluid Mech. 59 (1973), pp. 665–672.

[11] K.K. Ahuja and W.H. Brown, *Shear flow control by mechanical tabs*, AIAA paper 89-0094.

[12] L.J.S. Bradbury and A.H. Khadem, *The distortion of a jet by tabs*, J. Fluid Mech. 70 (1975), pp. 801–813.

[13] K.B.M.Q. Zaman, *Axis switching and spreading of an asymmetric jet: The role of coherent structure dynamics*, J. Fluid Mech. 316 (1996), pp. 1–27.

[14] L.P. Chua, S.C.M. Yu, and X.K. Wang, *Flow visualization and measurements of a square jet with mixing tabs*, Exper. Thermal Fluid Sci. 27 (2003), pp. 731–744.

[15] S.B. Verma, L. Venkatkrishnan, and G. Ramesh, *2-D PIV study of near-field flow development from a 2:1 elliptic jet with tabs,* AIAA paper 2007-4498.

[16] H.K. Tanna, *An experimental study of jet noise, Part II: Shock associated noise*, J. Sound Vib. 50 (1977), pp 429–444.

[17] T.D. Norum and J.M. Seiner, *Broadband shock associated noise from supersonic jets*, AIAA J. 20(1) (1982), pp. 68–73.

[18] A. Krothapalli, D.P. Wishart, and M.G. Mungal, *Supersonic jet control via point disturbances inside the nozzle*, AIAA J. 31(7) (1993), pp. 1340–1341.

[19] K.B.M.Q. Zaman, M.F. Reeder, and M. Samimy, *Control of an axisymmetric jet using vortex generators,* Phys. Fluids 6(2) (1994), pp. 778–793.

[20] P. Behrouzi and J.J. McGuirk, *Effect of tab parameters on near-field jet plume development*, AIAA J. Propul. Power 22(3) (2006), pp. 576–585.

[21] M.F. Reeder and M. Samimy, *The evolution of a jet with vortex real-time visualization and quantitative measurements*, J. Fluid Mech. 311 (1996), pp. 73–118.

[22] W.J. Gretta and C.R. Smith, *The flow structure and statistics of a passive mixing tab*, J. Fluids Eng. 115 (1993, June), pp. 255–263.

[23] S. Dong and H. Meng, *Flow past a trapezoidal tab*, J. Fluid Mech. 510 (2004), pp. 219–242.

[24] C.-W. Park and S.-J. Lee, *Flow structure around a finite circular cylinder embedded in various atmospheric boundary layers*, Fluid Dyn. Res. 30(4) (2002), pp. 197–215.

[25] R.J. Pattenden, N.W. Bressloff, S. R. Turnock, and X. Zhang, *Unsteady simulations of the flow around a short surface-mounted cylinder*, Int. J. Numer. Meth. Fluids 53 (2007), pp. 895–914.

[26] H. Wang, Y. Zhou, C. Chan, and T. Zhou, *Momentum and heat transport in a finite-length cylinder wake*, Exper. Fluids 46 (2009), pp. 1173–1185.

[27] C.T. Crowe, J.N. Chung, and T.R. Troutt, *Particle mixing in free shear flows*, Progr. Energy Combust. Sci. 14 (1988), pp. 171–194.

[28] L. Lourenco and A. Krothapalli, *On the accuracy of velocity and vorticity measurements with PIV*, Exper. Fluids 18 (1995), pp. 421–428.

[29] F.E. Jorgensen, *Directional sensitivity of wire and fibre-film probes*, DISA Inf. 11 (1971), pp. 31–37.

[30] J. Anderson, *Fundamental of Aerodynamics*, 4th ed., McGraw Hill, New Delhi, SIE, pp. 474–475.
[31] L.P. Bernal and A. Roshko, *Streamwise vortex structure in plane mixing layers*, J. Fluid Mech. 170 (1986), pp. 499–525.
[32] H.S. Husain and F. Hussain, *Elliptic jets, Part 3: Dynamics of preferred mode coherent structures*, J. Fluid Mech. 248 (1993), pp. 315–361.
[33] T.H. New, *An experimental study on jets issuing from elliptic inclined nozzles*, Exper. Fluids 46 (2009), pp. 1139–1156.
[34] T. Kawamura, M. Hiwada, T. Hibino, I. Mabuchi, and M. Kumada, *Flow around a finite circular cylinder on a flat plate*, Bull. JSME 27 (1984), pp. 2142–2151.
[35] F. Etzold and H. Fiedler, *The near-wake structure of a cantilevered cylinder in cross-flow*, Z. Flugwiss. 24 (1976), pp. 77–82.
[36] C.W. Park and S.J. Lee, *Free-end effects on the near wake flow structure behind a finite circular cylinder*, J Wind Eng. Ind. Aerodyn. 88 (2000), pp. 231–246.
[37] D. Sumner, J.L. Heseltine, and O.J.P. Dansereau, *Wake structure of a finite circular cylinder of small aspect ratio*, Exper. Fluids 37 (2004), pp. 720–730.
[38] H. Hui, T. Kobayashi, S. Wu, and G. Shen, *Changes to the vortical and turbulent structure of jet flows due to mechanical tabs*, Proc. Inst. Mech. Eng. Part C 213 (1998), pp. 321–329.